Molecular Crystals and Liquid Crystals

Publication details, including instructions for authors and subscription information:
http://www.tandfonline.com/loi/gmcl20

The Influence of Molecular Recognition on the Hydration of AG-013958 in the Solid State

T. E. Alcacio [a] , A. Sistla [a b] , T. Hsieh [b] & T. J. Thamann [c]

[a] Pfizer Global Research & Development, Department of Analytical Research & Development, San Diego, CA

[b] Thomas J. Long School of Pharmacy and Health Sciences, University of the Pacific, Stockton, CA

[c] Pfizer Global Research & Development, Division of Pharmaceutical Sciences, Kalamazoo, MI

Version of record first published: 21 Dec 2006

To cite this article: T. E. Alcacio, A. Sistla, T. Hsieh & T. J. Thamann (2006): The Influence of Molecular Recognition on the Hydration of AG-013958 in the Solid State, Molecular Crystals and Liquid Crystals, 456:1, 117-131

To link to this article: http://dx.doi.org/10.1080/15421400600788609

Mol. Cryst. Liq. Cryst., Vol. 456, pp. 117–131, 2006

ISSN: 1542-1406 print/1563-5287 online
DOI: 10.1080/15421400600788609

The Influence of Molecular Recognition on the Hydration of AG-013958 in the Solid State

T. E. Alcacio
A. Sistla
Pfizer Global Research & Development, Department of Analytical Research & Development, San Diego, CA

T. Hsieh
Pfizer Global Research & Development, Department of Analytical Research & Development, San Diego, CA and Thomas J. Long School of Pharmacy and Health Sciences, University of the Pacific, Stockton, CA

T. J. Thamann
Pfizer Global Research & Development, Division of Pharmaceutical Sciences, Kalamazoo, MI

In the solid state, AG-013958 exists as a three-dimensional hydrate that dehydrates completely at 109°C with subsequent melting at 183°C. Water molecules in the AG-013958 crystal structure occupy hydrophilic sites and anchor neighboring drug molecules through H bonding. Because hydrates/dehydrates display different physical properties related to dissolution, solubility & bioavailability, the stability of AG-013958 monohydrate was investigated. A reversible hydration/dehydration of AG-013958 was observed in which a meta-stable dehydrate was created on removal of H_2O. Solid-state x-ray diffraction data suggest the reversible hydration mechanism results from molecular recognition between drug molecules, which affects molecular packing and the observed channel network. The hydration rate was largely dependent upon vapor pressure and the rate of hydration doubled from 7.6 to 15% R_H at ambient conditions, whereas temperature influenced the hydration kinetics to a much lesser extent. Hydrate stability can be controlled by maintaining pharmaceutical processing conditions at $R_H \geq$ 15% at 25°C.

Keywords: hydrate; mechanism; pharmaceutical; reversible; solid; vapor pressure

The authors would like to thank Alan Deese for performing SS-NMR. This manuscript is dedicated to the memory of Prof. Dale E. Sayers.

Address correspondence to A. Sistla, Pfizer Global Research & Development, Department of Analytical Research & Development, San Diego, CA 92121, USA. E-mail: asistla@pfizer.com

INTRODUCTION

AG-013958 hinders tyrosine kinase activity of VEGF receptors and retinal neovascularization (formation of new blood vessels), which cause scarring in the macula region of eye leading to eventual blindness [1]. Under ambient conditions, AG-013958 exists as a hydrate. However, the hydrate undergoes dehydration around 109°C with a subsequent melt at 183°C which is the anhydrous melting point. Changes in the hydrated state of pharmaceutical solids are known to affect physicochemical properties such as solubility [2], dissolution [3], bioavailability [4], compaction [5], flowability, and tableting [6]. Therefore, hydrate formation and handling represent important challenges. Hydrates can exist as stoichiometric or non-stoichiometric hydrates, as discreet, channel, or planar hydrates [7]. In addition, hydrates may undergo partial, irreversible, or reversible phase changes over different temperatures [8]. The antibacterial agent Cephradine is one example in which both the mono and dihydrate undergo irreversible conversion when dehydrated with collapse of the crystal structure to an amorphous phase [9]. With other molecules such as Thymine monohydrate, spatially oriented dehydration occurs along a specific axis leaving the original unit cell intact but with lower density due to voids created by vacated water [10]. The number of possible hydrate structural environments and frequency of occurrence in the organic solid state has been surmised [11,12]; however further studies are needed to analyze factors at the molecular level that affect hydration from a mechanistic standpoint [13].

In this study, we have defined the molecular environment of the solid state and have attempted to understand how the determined environment impacts hydration and crystal structure. In addition, critical variables that affects hydration and can be used to monitor the bulk state are described.

MATERIALS AND METHODS

AG-013958 monohydrate was obtained from Chemical Research & Development, Pfizer-La Jolla (Fig. 1). The AG-013958 dehydrate was produced by heating the monohydrate at 100°C under vacuum for 1 hr. The sample was removed from the vaccum oven and allowed to cool to ambient temperature (18 to 22°C) in a P_2O_5 desiccator. Powder x-ray diffraction pattern data was collected using a Discover D8 GADDS diffractometer (Bruker, Madison W.I.) using copper Kα radiation (40 kv, 40 mV). Data was collected from 4 to 40° 2θ at a step size of 0.02° and step time of 60 seconds.

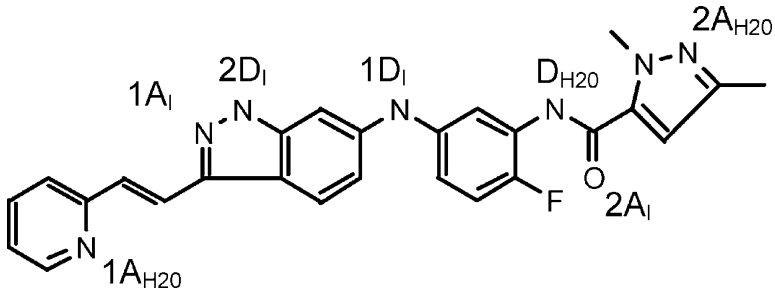

FIGURE 1 Line drawing of the AG-013958 molecule. H donor (D_{H_2O}) and acceptor (A_{H_2O}) sites involved with H_2O are noted, as well as donor (D_I) and acceptor (A_I) sites involved in complimentary *intermolecular* associations.

Thermal Analysis

Differential scanning calorimetry (DSC) and thermogravimetry analysis (TGA) were performed to characterize thermal events and the weight loss profile of samples. A DSC Q1000 and TGA Q500 were utilized (TA Instruments, New Castle D.E.) in which samples were heated at 10°C per minute. For DSC experiments, an Indium standard (mp 157°C) was used to calibrate the DSC instrument while the system was continuously purged with nitrogen at 40 ml min^{-1}. Approximately three milligrams of AG-013958 sample was used for measurement.

Vapor Sorption Experiments

Gravimetric vapor sorption experiments were carried out with a DVS-1000 (Surface Measurement Systems). Approximately 15 mgs of dehydrate AG-013958 was used for each measurement. Two main types of experiments were performed. First, water sorption experiments were carried out by measuring weight increases at constant vapor pressure (V_p) – 3.56 torr at 25, 35, 40, and 45°C. The second set of experiments involved measuring water sorption at constant temp (30°C) at 7.6, 11.2, 15, and 19% relative humidity (R_H). To ensure accurate measurements, calibrations were performed at each temperature point at 0% R_H with an aluminum 100 mg standard. PXRD data were also collected on samples stored in the DVS chamber at 0% R_H for $\sim$16 hours to ensure the initial DVS step would maintain the dehydrated state ad infinitum.

Single Crystal Structure Determination

Single crystals of AG-013958 were generated by dissolving 15 mg of compound into 3 mL of DMSO. The solution was filtered (Milipore, 0.2 μm) into a Wheaton glass 25 mL scintillation vial, and the cap was slightly tightened. After 6 weeks, a colorless plate formed. The single crystal was washed with ethanol, dried under ambient conditions, and mounted on the end of a glass 0.1 mm fiber. Data were collected with a Bruker D8 SMART Apex CCD equipped with a graphite-monochomated Mo Kα (0.71073 Å) sealed tube x-ray source. Data were collected at RT using a series of ω and ψ scans (0.3° frame width), and the initial cell was indexed with SMART software v.5.626 (Bruker, Madison W.I.). Data integration and final cell assignment were performed with SAINT v. 6.36a (Bruker, Madison W.I.). Multi scans absorption corrections were applied with SAINTABS (Bruker, Madison W.I.). A trial structure was obtained with direct methods and refined against F^2 on 11,913 reflections. A difference map revealed a water of crystallization. Hydrogen positions were calculated wherever possible. The methyl hydrogens and the hydrogens on nitrogen and oxygen were located by difference Fourier techniques. The final R-index was 6.86%. Supplementary crystallographic data for the AG-013958 crystal can be obtained free of charge from The Cambridge Crystallographic Data Centre by requesting number *297503* via www.ccdc.cam.ac.uk/data_request/cif."

Variable Temperature PXRD

Variable thermal PXRD (VT-PXRD) data were collected using a Eularian cradle variable temperature chamber (MRI, Karlsruhe FRG) mounted on a Bruker GADDS D8 Discover diffractometer. Hydrated samples were heated on the temperature stage at 10°C per minute to 25, 80, 100, 110 and 120°C, and held for 2 minutes prior to data collection.

Raman Spectroscopy

Raman spectroscopic studies were performed using a Kaiser RXN1e spectrometer with 785-nm irradiation. Cyclohexane was used as a wavelength standard. A continuous sampling mode was used in which data was collected every 9 seconds – one dark frame followed by two 3 second exposures. The data was background-subtracted and averaged.

Solid State NMR

Solid-State ^{13}C NMR spectroscopy was performed on hydrated and dehydrated samples. Samples were packed in 4 mm outer diameter ZrO_2 rotors. The dehydrated sample was prepared by heating at 100°C for 16 h *in vacco*, and immediately capped with a Kel-F top to minimize moisture uptake. The sample was spun at 12 kHz in a standard Bruker broad band CPMAS probe and spectra were recorded at 150.91 MHz on a Bruker Avance 600 spectrometer (Bruker, Billerica, MA.). The static field homogeneity was shimmed for ^{13}C line widths in adamantane of 2 Hz (full width at half-height). Two-pulse phase modulation (TPPM) proton decoupling was used during signal acquisition with 100 kHz RF amplitude, 5 μs pulse width, and a phase difference of 15° between two successive pulses. A cross polarization contact time of 2 ms and a recycle delay of 5 s were used. Chemical shifts were externally referenced to the methyl resonance of hexamethyl benzene at 17.36 ppm.

RESULTS AND DISCUSSION

In the solid state, AG-013958 exists as a monohydrate as evidenced from the DSC & TGA data. This stoichiometry as determined by the TGA data indicated 3.8% mass was lost when the sample was heated and 109°C (Fig. 2). This loss of mass was equivalent to one H_2O

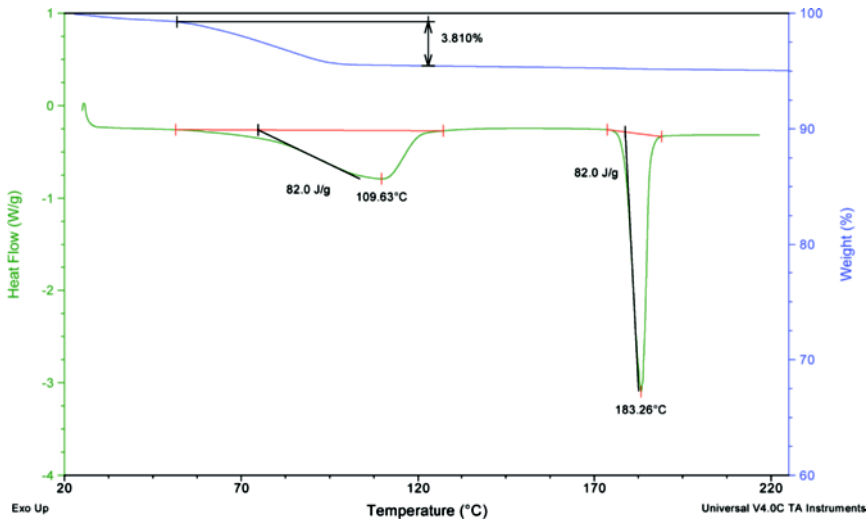

FIGURE 2 DSC and TGA trace of AG-013958 monohydrate.

molecule. Complimentary DSC measurements of hydrated samples displayed an endotherm onset commencing at 82°C, and reaching a minimum in heat flow at 109°C. The endotherm, coupled with the loss of mass equivalent to one H_2O molecule, suggested the observed thermal event most likely resulted from dehydration. The endothermic event yielded a dehydration energy of 82 J/g with a dehydrate melt at 184°C (87 J/g). Contributions to the dehydration endotherm most likely involve energetics from breaking H bonds between drug and water molecules. DSC measurements yield an average H bond energy of 10 kcal mole^{-1} which compared favorably to published values [14].

The PXRD data of this AG-013958 monohydrate showed distinct changes in the diffraction pattern following exposure to 100°C *in vaccuo* for 1 h (Fig. 3). In particular, diffraction peaks at 11.8, 12.0, and 23.5° 2θ were apparent and indicated changes to the crystal structure. HPLC results indicated that the change was not a result of degradation as the parent molecule was retained. Karl Fisher analysis of the dehydrate showed 0.6% water was present which was equivalent to a loss of 85% of initial water. The Karl Fisher and PXRD data indicate changes in crystal structure resulted from dehydration.

The phase boundaries of the hydrate/dehyrdrate were further resolved with VT-PXRD. The monohydrate was stable between 80 and 90°C, however a phase change was detected when holding the temperature ≥100°C, as significant increases in diffraction intensities

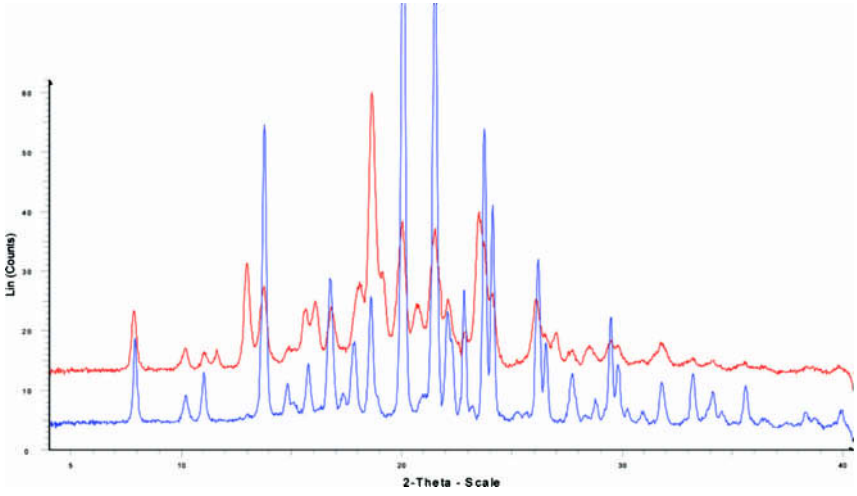

FIGURE 3 PXRD of AG-013958 – bottom to top. Monohydrate, dehydrate after 1 h 100°C *in vacco*.

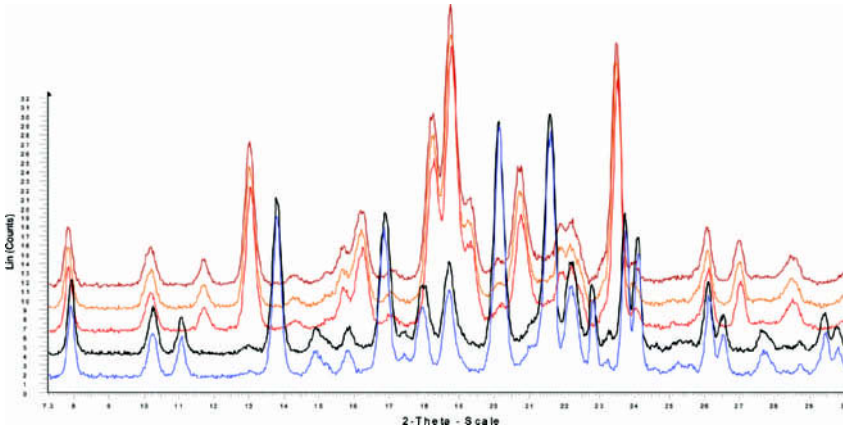

FIGURE 4 Variable temperature PXRD of AG-013958, monohydrate. Bottom to top: 25, 80, 100, 110, and 120°C.

were observed at 11.8, 12.0, and 23.5° 2θ (Fig. 4). When comparing the PXRD data for the anhydrous form in Figure 3 to that in Figure 3, it was apparent that some rehydration had occurred. In Figure 3, the dehydrated sample displayed a significant number of hydrate peaks at 11.0 13.8, 17.0, 20.0, and 21.5° 2θ that were not found in Figure 4. This result demonstrated hydration was a reversible process in which samples rehydrate upon removal from a vacuum and when allowed to cool below 100°C.

When examining the VT-PXRD data collected at ≥100°C in closer detail, low angle reflections at 7.8 and 10.3° 2θ were also observed in the fully dehydrated sample (Fig. 4). These low angle reflections result from long-range periodicity of the solid state. In the hydrate structure, this diffraction corresponds to the (011) and (100) miller indices – specifically slices perpendicular and parallel to *a*, along and diagonal to *bc* unit cell axis, respectively. The similar '*d*' spacing produced from reflections in both the hydrate and dehydrate suggest aspects of the monohydrate crystal packing were retained after removal of entrapped water. Similar findings have been reported with Erythromyacin dihydrate, where the dehydration increased crystal packing between 2.6 to 5.2% [15] yet maintained the overall long range order & space group. Solid state NMR results of the dehydrate crystal indicated short range order changes result from local conformational variations did occur [16]. In the case of AG-013958, our ability to determine the crystalline space group was less certain as significant changes were observed in the PXRD of the dehydrate. Nonetheless,

the dehydration reaction can be considered topotactic as at least one orientation in the daughter cell share crystallographic equivalence with the parent monhydrate [17].

Due to the fact that rehydration may occur rapidly, other methods were utilized to understand the rehydration phenomena. We were interested in studying the dynamics of the hydration process, specifically how the chemical environment was affected by the dehydration process, and how the dehydrate differed from the hydrated solid state. Raman spectroscopy was utilized given this method is amenable to studying long range differences in the solid state derived from the inelastic scattering of photons, and provides local molecular information resulting from vibrations that occur due to chemical changes. We observed that the Raman spectra for both the hydrate and dehydrated samples were similar (Fig. 5), supporting the hypothesis that the dehydrate contains similar long-range order as the hydrated molecule. However, a few spectral differences were apparent between the two data sets. Upon dehydration, there is an increase in the amide I carbonyl stretching frequency from 1650 to 1658 cm^{-1} [18]. There is also a small shift in the amide II N–H bending mode near 1520 cm^{-1}. Other noticeable differences between the hydrate and dehydrate were observed at approximately 1000 cm^{-1}. For the hydrate, a single band at 1003 cm^{-1} was found while the dehydrate displayed an additional lower frequency band at 992 cm^{-1}. After exposing

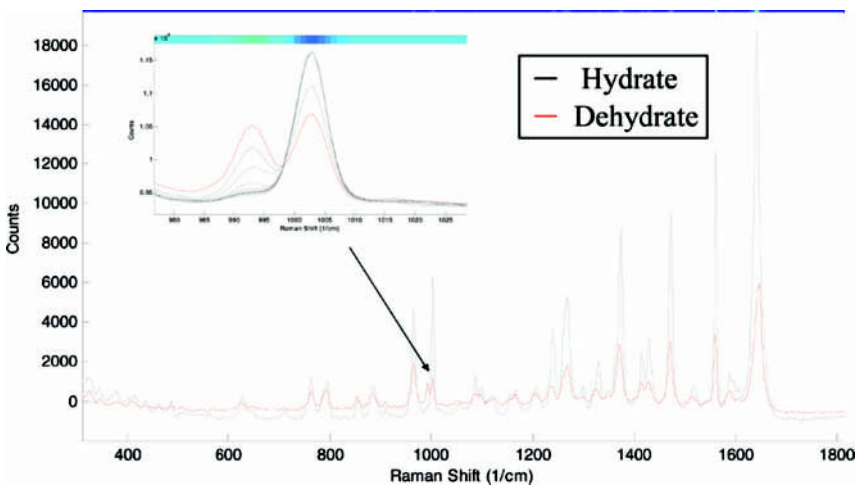

FIGURE 5 Raman Spectra of AG-013958 dehydrate (red) and hydrate (grey). Inset – Spectra of the dehydrate over a 34 minutes period while being exposed to ambient conditions.

the dehydrate to normal lab humidity, the lower frequency band at 992 cm^{-1} disappeared and the spectra mirrored that of the original hydrate within 34 minutes. The reversibility of the Raman data throughout the hydration/dehydration cycle indicates a recognition pattern exists for water molecules to re-enter and consistently occupy defined positions in the intermolecular channel. Although an unequivocal assignment of the vibrations are difficult, the Raman shifts may result from the symmetric ring breathing mode of the 2-substituted pyridine ring [19]. Raman data suggest both the pyridine and amide group were involved in hydrogen bonding in the hydrate. Interaction with water would certainly affect the vibrational frequencies of donor and acceptor atoms in these groups.

To gain additional evidence and understand the factors that influence the hydration reversibility, we utilized ^{13}C solid state NMR. In addition to providing complimentary solid state information, ^{13}C SS-NMR is highly sensitive to local chemical changes [20]. The NMR spectra for the hydrate and dehydrate showed clear differences. For example, the hydrate exhibited methyl peaks δ values of 16.5 and 39 ppm that shifted downfield upon dehydration (Fig. 6). The SS-NMR data indicated the pyrazole region of the molecule was sensitive to the presence/absence of water (Fig. 5). Dehydration may influence the

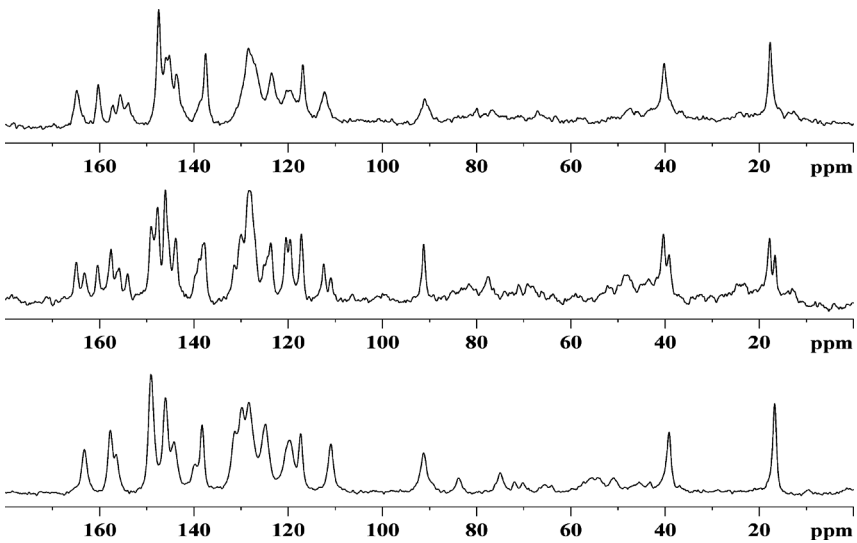

FIGURE 6 ^{13}C SS-NMR of AG-013958 monohydrate. Bottom to top. Samples equilibrated under ambient conditions, 100°C for 16 h with 2 min exposure to ambient conditions, 100°C for 16 no ambient exposure.

chemical environment in several ways. Chemical changes may result from variations involving the aforementioned groups by either a direct association with water molecules through hydrogen bonding, or through intermolecular bonding between adjacent drug molecules, or indirectly through nearest neighboring atom chemical changes. Methyl groups can act as weak H bond acceptors for intermolecular bonding motifs [21], however, changes in methyl shifts typically result from the proximity to other H bond donors/acceptors. In the AG-013058 molecule, both methyl carbons branch from a pyrazole residue and occupy neighboring positions to a nitrogen within this heterocyclic ring. The down field shifts that result from the pyrazole residue suggest the N atom may serve as nucleophilic site and accept H bonds from water molecules. In addition to methyl signals detected by SS-NMR, the amide-carbonyl δ signal at 165 ppm was detected and shifted downfield with dehydration. This finding was consistent with observations from the Raman spectra which showed an increase in the amide I carbonyl stretching frequency with dehydration. Carbonyls have a greater probability in acting as hydrogen bond acceptors. The increase in carbonyl stretching frequency upon dehydration is unusual, as one would expect greater molecular loosening from voids created by vacated water [18]. This increase in carbonyl stretching suggests other binding modes may be present which have not been considered.

Finally, to better understand the H bond assignments of the hydrate, small molecule x-ray diffraction was used to probe the possibility of intermolecular interactions. Crystallographic analysis of the AG-013958 single crystal demonstrated a 1:1 drug to water stoichiometry (Table 1) that concurred with previous TGA data. Closer analysis of the P21C monoclinic structure indicated the presence of uniform channels traversing the unit cell. The channels result largely from preferred packing created by intermolecular H bonding between adjacent drug molecules (Fig. 6). Using graph set analysis [22], the supramolecular motif made up of C_1^1 chains play an important role in affecting hydration properties. The complimentary motif forms a di-molecular zipper where teeth at one end are comprised of intermolecular bonding involving benzimidazole N–H – carbonyl (2.20 Å) and benzimidazole N – secondary amine linkages (2.01 Å). At the other end of the intermolecular association, a hydrophilic domain is formed where water bond with 3 different drug molecules. Hydration sites are symmetry equivalent and display three-fold coordination – two H acceptors (N–(H_2O), 1.855 (pyridine) and 2.091 Å (pyrazole) and one donor (NH–(OH_2), 2.025 Å amide). Three-fold coordination involving water is the most common type of bonding environment in the hydrated organic solid state [23]. Given the extended but tortuous

TABLE 1 Crystal Refinement Data for AG-013958

Experimental formula	$C_{26}H_{22}N_7OF \cdot H_2O$
Formula weight	485.52
Crystal dim (mm^3)	$0.20 \times 0.25 \times 0.35$
Crystal system	Monoclinic
Space group	P2(1)/c
a (Å)	8.7014(10)
b (Å)	19.986(2)
c (Å)	13.6360(15)
V ($Å^3$)	2370.3(5)
Z	4
ρ ($g\,cm^{-3}$)	1.361
T (K)	298(2)
F_{000}	1016
# of indep refl.	2476
# of variables	345
R (F_o)	0.0686
R_w (F_o^2)	0.2098
Goodness of fit	1.209

channel network fixed by the supramolecular synthon, water can enter/exit isolated cavities and connected channels with small changes in environmental conditions. Upon dehydration, an increase in the carbonyl stretching frequency was observed and suggested the C_1^1 synthon was conserved upon dehydration. Recall from the VT-PXRD, the *a* axial unit cell length in the dehydrate was comparable to the monohydrate based on similar diffraction intensities and positions for (100) plane. Closer inspection of the (100) demonstrated that this plane repeatedly dissects intermolecular rings that contain the carbonyl moiety (Fig. 7). Although dehydration clearly causes conformational changes as demonstrated by the chemical shifts particularly from the pyrazole and pyidine; these changes were offset by comparable dimension in the dehydrate *a* axis affected by carbonyl binding in the C_1^1 synthon. A complete collapse of the crystal is not expected, as carbonyl H bonding act as a cohesive force and limits the degree of disassociation.

Bulk Property Assessment

We were interested in how the molecular properties affected properties of the bulk, such as the stability of the dehydrate, the ability to gain crystalline water, and the rate at which water uptake would occur, to determine whether the dehydrate could be used for manufacturing. Upon exposing the dehydrate at 30°C to relative humidity levels ranging from 7.6 to 19%, $\sim$1 equivalent of H_2O was taken up (Fig. 8). The rate of hydration was highly dependent on the relative humidity,

FIGURE 7 A 3D representation of the AG-013958 monohydrate. The hydrophilic cavity is shown where H bonding occurs with 3 distinct molecules. This binding site results from the complimentary C_1^1 drug-drug association shown to the right side, with bond distances of 2.013 and 2.200 Å.

as hydration rates increased from 7.6 to 19% R_H. To reach equilibrium and regain an equivalent of H_2O, 200 minutes were required at 7.6% R_H while only 99 minutes were needed at 15% R_H.

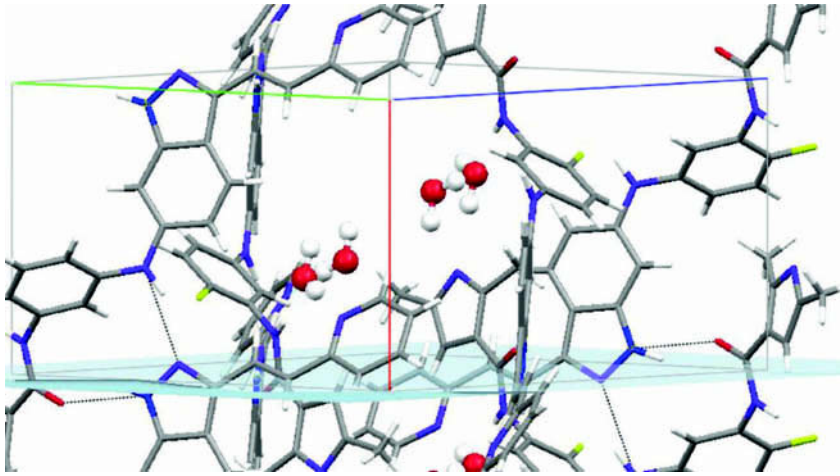

FIGURE 8 Packing diagram of the AG-013958 monohydrate showing the unit cell and 100 plane. The crystalline stability at high temperature and hydration reversibility results from the C_1^1 intermolecular motif dissected by the 100 plane.

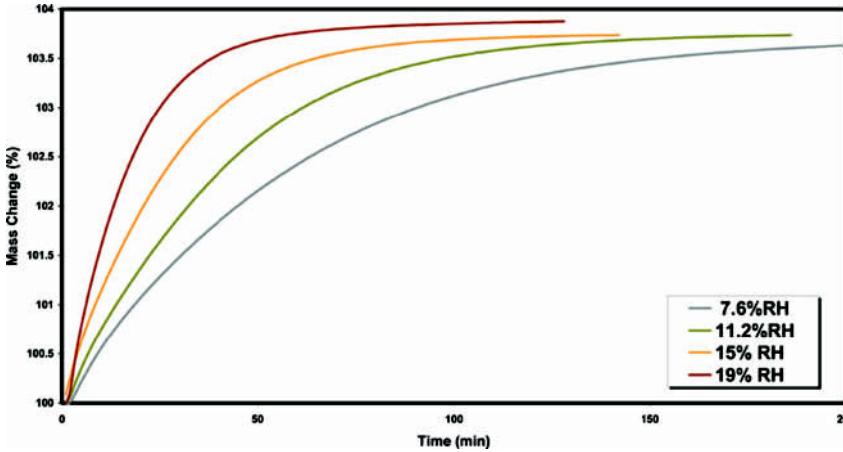

FIGURE 9 Kinetic water vapor sorption on AG-013958 dehydrate at RT. From bottom to top: 7.6, 11.2, 15, and 19% R_H.

To understand which conditions had the greatest influence on the hydration process, several kinetic experiments were carried out in which both temperature and vapor pressure were systematically varied (Fig. 9). In addition, models that included zero order kinetics, phase boundary diffusion, and random nucleation were employed to determine the hydration mechanism [24]. The random nucleation model in particular fit the entire data set best over other geometric models (Table 2). Using the random nucleation model, the rate of hydration for variations in temperature and relative humidity was derived. These hydration curves are depicted in Figure 10. At a constant temperature of 30°C, the hydration rate doubled from 0.28 min^{-1}

TABLE 2 Best Fit Indices Derived from Plotting Data Generated from Figure 8 to Various Solid State Mechanistic Models

Equation	Expression	7.6% R_H	11% R_H	15% R_H	19% R_H
Zero-order mechanism	$\alpha = kt$	0.840	0.750	0.693	0.655
Phase boundary, cylindrical symmetry	$1-(1-\alpha)^{1/2} = kt$	0.972	0.926	0.892	0.858
Phase boundary, spherical symmetry	$1-(1-\alpha)^{1/3} = kt$	0.995	0.974	0.954	0.921
Random nucleation	$(-\ln(1-\alpha)) = kt$	0.994	0.998	0.999	0.991
Random nucleation, 2D growth	$(-\ln(1-\alpha))^{1/2} = kt$	0.996	0.990	0.988	0.969
Random nucleation, 3D growth	$(-\ln(1-\alpha))^{1/3} = kt$	0.987	0.978	0.972	0.965

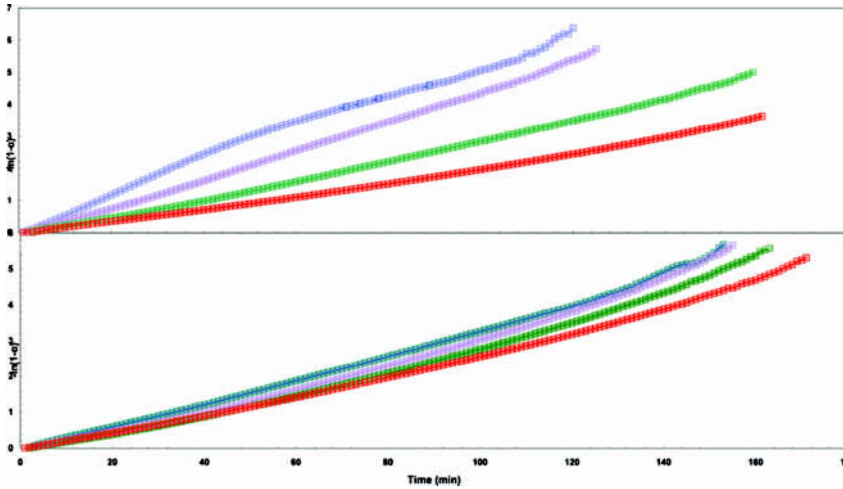

FIGURE 10 Random nucleation model of AG-013958 dehydrate vapor sorption as a function of R_H (top) and temperature (bottom). Upper plot – from bottom to top: 7.6, 11, 15, and 19% R_H at 30°C. Lower plot – from bottom to top: 45, 40, 35, and 25°C at 3.56 Torr.

at 7.6% R_H to 0.046 min^{-1} at 15% R_H. The hydration rate leveled at 15% R_H as evidenced by a similar rate (0.047 min^{-1}) observed at 19% R_H. When holding the vapor pressure at 3.56 Torr and increasing temperature from 25 to 45°C, a decrease in the hydration rate of 11% was observed. Ono *et al*. [25] also observed dehydration rates decreased slightly with increasing temperature with carbamazepine. Therefore, the influence of temperature on the hydration rate was significantly less than compared to relative humidity. This finding of course applies only to ambient conditions, as temperatures $\geq$100°C will affect a phase change as evidenced by the VT-PXRD studies.

CONCLUSION

In the solid state, AG-013958 forms a three-dimensional hydrate structure that dehydrates completely at 109°C with subsequent melting at 183°C. Water molecules may easily enter/exit the crystalline lattice due to an extensive pore network created from intermolecular bonding between adjacent drug molecules. The intermolecular bonding also creates specific symmetry equivalent hydration sites in which water binds 3 drug molecules. Upon dehydration, local disorder occurs yet some long range order is retained, particularly parallel to

the *a* axis and along the *bc* diagonal. The C_1^1 supramolecular motif is expected to play an important role in regulating solid to solid phase transitions upon dehydration, enabling a reversible hydration reaction. To sustain hydrate stability, processing conditions should be maintained at $R_H \geq$ to 15% at 25°C to take advantage of the higher rates of hydration.

REFERENCES

[1] Clark, A. F. & Yorio, T. (2003). *Nature Rev*., *2*, 448.
[2] Pudipeddi, M. & Serajuddin, A. T. M. (2005). *J. Pharm. Sci*., *94*, 929.
[3] De Smidt, J. H., Fokkens, J. G., Grijseels, H., & Crommelin Daan, J. A. (1986). *J. Pharm. Sci*., *75*, 497.
[4] Poole, J. W., Owen, G., Silverio, J., Freyhof, J. N., & Roseman, S. B. (1968). *Curr. Ther. Res. Clin. Exp*., *10*, 292.
[5] Smita, D. & Suryanarayanan, R. (2004). *AAPS Pharm. Sci. Tech*., *5*, 1.
[6] Bauer, J. F., Dziki, W., & Quick, J. E. (1999). *J. Pharm. Sci.*, *88*, 1222.
[7] Morris, K. R. (1998). Structural characteristics of crystalline hydrates. In: *Polymorphs in Pharmaceutical Solids*, Brittain, H. G. (Ed.), Marcel Dekker: New York, 125.
[8] Vippagunta, S. R., Brittain, H. G., & Grant, D. J. W. (2001). *Advanced Drug Delivery Reviews*, *48*, 3.
[9] Florey, K. & Florey, C. K. (ed) (1972). *Analytical Profiles of Drug Substances*, *1*, 367.
[10] Perrier, P. & Byrn, S. (1982). *J. Org. Chem*., *47*, 4761.
[11] Steiner, T. & Saenger, W. (1993). *J. Amer. Chem. Soc*., *115*, 4540.
[12] Infantes, L. L., Chisholm, J., & Motherwell, S. (2003). *Cryst. Eng. Comm.*, *5*, 480.
[13] Gillon, A. L., Davey, R. J., Storey, R., Feeder, N., Nichols, G., Dent, G., & Apperley, D. C. (2005). *J. Phys. Chem. B*, *109*, 5341.
[14] Desiraju, G. R. & Steiner, T. (1999). *The Weak Hydrogen Bond in Structural Chemistry*, IUCr. Oxford University Press: New York.
[15] Stephenson, G. A., Groleau, E. G., Kleemann, R., Xu, W., & Rigsbee, A. (1998). *J. Pharm. Sci.*, *87*, 536.
[16] Stephenson, G. A., Stowell, J., Toma, P., Pfeiffer, R. R., & Byrn, S. (1997). *J. Pharm. Sci.*, *86*, 1239.
[17] Galeway, A. K. (2000). *Thermochim. Acta*, *355*, 181.
[18] Triggs, N. E. & Valentini, J. J. (1992). *J. Phys. Chem*., *96*, 6922.
[19] Klots, T. D. (1998). *Spectrochim. Acta*, *54*, 1481.
[20] Te, R. L., Griesser, U. J., Morris, K. R., Byrn, S. R., & Stowell, J. G. (2003). *Cryst. Growth & Des*., *3*, 997.
[21] Shimon, L. J. W., Vaida, M., Addaddi, L., Lahav, M., & Leiserowitz, L. (1990). *J. Amer. Chem. Soc.*, *80*, 6215.
[22] Bernstein, J., Davis, R. E., Shimoni, L., & Chang, N. L. (1995). *Angew. Chem. Int. Ed. Engl.*, *34*, 1555.
[23] Gillon, A. L., Feeder, N., Davey, R. J., & Storey, R. (2003). *Cryst. Growth & Des.*, *3*, 663.
[24] Sharp, J. H., Bridley, G. W., & Narahari Achar, B. N. (1966). *J. Am. Ceramic Soc.*, *49*, 369.
[25] Ono, M., Tozuka, Y., Oguchi, T., Yamamura, S., & Yamamoto, K. (2002). *Int. J. Pharm.*, *239*, 1–12.